buildings

MDPI

Article

Swelling Behavior and Flow Rates of a Novel Hydrophilic Gasket Used in Composite Geomembrane Vertical Cutoff Walls and Infrastructures Exposed to Contaminated Groundwater

Min Wang, Xianlei Fu, Zheyuan Jiang, Chi Che, Ningjun Jiang and Yanjun Du *

Jiangsu Key Laboratory of Urban Underground Engineering & Environmental Safety, Institute of Geotechnical Engineering, Southeast University, Nanjing 210096, China
* Correspondence: duyanjun@seu.edu.cn

Abstract: The swelling capacity of novel hydrophilic gaskets used in geomembrane cutoff walls and infrastructures is critical for decreasing the flow rates of contaminated groundwater. This study investigated the swelling behavior, relaxation characteristics, flow rates, and micro-morphology of a hydrophilic gasket with different testing liquids. The radial swelling tests were performed using a device modified from single-lever consolidation instrument. A flow rates model apparatus was manufactured and employed to measure the flow rates of the poor-sealing hydrophilic gasket. According to the test results, the swelling ratio of the hydrophilic gaskets soaked in the DIW were the highest, followed by the NaCl solution, the MSW landfill leachate, and the $CaCl_2$ solution. Relaxation phenomena appeared in all the specimens regardless of the testing liquids. The flow rates of the specimens penetrated with DIW, NaCl, and $CaCl_2$ decreased to a stable state, and then increased extremely slowly to stable values. Moreover, self-healing of the hydrophilic gasket was observed. The micro-morphology indicated that sodium polyacrylate (PAAS) with insufficient expansion could separate from the matrix under high multivalent ionic strength or loading pressure conditions. Therefore, it is critical to develop the modified hydrophilic gasket with resistance to contaminated groundwater for a better barrier performance for use in contaminated sites and infrastructures.

Keywords: hydrophilic gasket; swelling ratio; model apparatus; flow rates; relaxation; sodium polyacrylate; microdamage

Citation: Wang, M.; Fu, X.; Jiang, Z.; Che, C.; Jiang, N.; Du, Y. Swelling Behavior and Flow Rates of a Novel Hydrophilic Gasket Used in Composite Geomembrane Vertical Cutoff Walls and Infrastructures Exposed to Contaminated Groundwater. *Buildings* **2022**, *12*, 2207. https://doi.org/10.3390/buildings12122207

Academic Editors: Siu-Kit Lau, Vesna Kosorić, Abel Tablada, Zdravko Trivic, Miljana Horvat, Milena Vukmirović, Silvia Domingo-Irigoyen, Marija Todorović, Jérôme H. Kaempf, Kosa Golić and Ana Peric

Received: 27 October 2022
Accepted: 5 December 2022
Published: 13 December 2022

1. Introduction

Vertical cutoff walls are often constructed to decrease the flow rates of contaminated groundwater at municipal solid waste (MSW) landfill and industrial sites [1–4]. Vertical cutoff walls are constructed using a mixed backfill of a composite material, such as soil–bentonite (SB), cement–bentonite (CB), or soil–slag–cement (SSC) [5,6]. However, concerns over the integrity of these vertical cutoff walls come about via (1) the improper mixing of slurry support and backfill materials, (2) defects in the joints and stoppages during construction, (3) the effects of dry–wet cycling or long-term desiccation on the backfill materials in unsaturated zones, (4) freeze–thaw behavior of vertical cutoff walls in northern climates, and (5) the hydraulic conductivity of the backfill materials exposed to contaminants [7]. Geomembranes used with SB, CB, and SSB backfill materials as a composite vertical cutoff wall are one way to solve the above problems, and they decrease the hydraulic conductivity [7,8]. Geomembranes have a long history of successful use in contaminated sites due to them being highly resistant to a variety of contaminations [6,7,9,10]. The researchers in [5,11] analyzed the hydraulic performance of a geomembrane composite vertical cutoff wall and compared it with a geomembrane vertical cutoff wall and an SB vertical cutoff wall. The results showed that the geomembrane composite vertical cutoff wall was widely recognized to provide lower flow rates than the geomembrane vertical cutoff wall or the SB vertical cutoff wall. A geomembrane with pre-welded interlocks,

hydrophilic gaskets, and backfill materials constitutes a complete composite vertical cutoff wall [12–14].

In order to reduce field welds, the interlocks are pre-welded to the geomembrane sheets (Figure 1a). A hydrophilic gasket may be injected into the joint during installation and expands when it comes in contact with liquids, which can be used to seal the joints [12]. One can create a geomembrane that is virtually impermeable, but the system will not function properly if the connections leak [7]. Without failing, hundreds of EPA 9090 compatibility tests on HDPE geomembranes were conducted with a range of municipal and hazardous leachates. Additionally, the strength and hydraulic qualities of the interlocks and hydrophilic gaskets are also crucial because they may be stressed during installation or if some lateral displacement or settlement takes place in the vertical cutoff walls [15]. The properties of interlocks, which are pre-welded to the geomembrane panels, are tested in the factory. Therefore, the joints are the primary cause for concern with regard to the use of geomembranes in vertical cutoff walls. [5,7,15]. For example, a hydrophilic gasket may be pulled off during installation. Additionally, the swelling behavior, self-healing, and sealing pressure of the hydrophilic gaskets are critical to the hydraulic performance of geomembrane composite vertical cutoff walls [15,16].

Novel hydrophilic gaskets, which were developed in the late 1970s, have been applied in underground facilities to prevent groundwater penetration for many years due to their elasticity, super water absorption capacity, and low permeability [17,18]. After water absorption, swelling is constrained, generating contact pressure between the expanded hydrophilic gasket and the interlocks. The sealing function of a hydrophilic gasket can be accomplished depending on this contact pressure [17,19]. The rubber matrix, hydrophilic materials, and additives are the components of a hydrophilic gasket. The properties of high elasticity, high strength, and effective aging resistance are necessary for a rubber matrix. Natural rubber [17,18,20], chlorinated polyethylene (CPE) [21,22], isobutylene rubber, chloroprene rubber (CR), chlorohydrin rubber, acrylonitrile rubber [20,23,24], ethylene propylene diene monomer (EPDM), silicon rubber, or vulcanized silicone rubber [25] are some of the most common hydrophobic rubbers used in hydrophilic gaskets. To make a hydrophilic gasket swell, super-absorbent polymer (SAP) is applied. SAP is a polymer electrolyte with a very extensive crosslinking network and a hydrophilic group [18,26]. It is capable to holding 1000 times its own weight in weight [27]. Additionally, it has exceptional water retention, allowing it to maintain water pressure. Numerous investigations have been conducted to determine how additives [18,20,28], rubber matrixes, SAP [17,29,30], compatibility agents [20], or micro-morphologies [31,32] affect a hydrophilic gasket's water swelling behavior and sealing abilities. Ren et al. [21] investigated the kinetics of the water swelling process of a hydrophilic gasket with different PAAS, additive contents, and temperature conditions. The results indicated that the mechanism underlying the water swelling process was not limited to Fickian diffusion and that the relaxation of the PAAS and CPE matrix chain had a significant impact on it. Nevertheless, geomembrane composite vertical cutoff walls are constructed in contaminated sites, which presents challenges due to the corrosive environment [10,16]. Furthermore, few studies have been performed on the swelling behavior and flow rates of hydrophilic gaskets under complex contaminated conditions involving heavy metals, MSW landfill leachates, and salt solutions. Additionally, compressive stress relaxation, which causes contact stress to diminish or even vanish over time [17,33,34], contributes to the failure of the hydrophilic gaskets. The sealing ability of hydrophilic gaskets cannot be maintained over time [35,36]. In order to estimate a hydrophilic gasket's service life in contaminated areas, it is required to also examine its relaxation characteristics. According to the aforementioned literature, the high flow rates caused by defects or failures of hydrophilic gaskets are summarized in Figure 1, including the low swelling ratio of a gasket contacted with contaminated groundwater, expansion–relaxation, and the fracture of a gasket caused during installation. Most researchers [7,13,15,16] have indicated that the resistance of hydrophilic gaskets used

in geomembrane composite cutoff walls to MSW, chemicals, tailing, and hazardous waste leachates is an area that requires investigation.

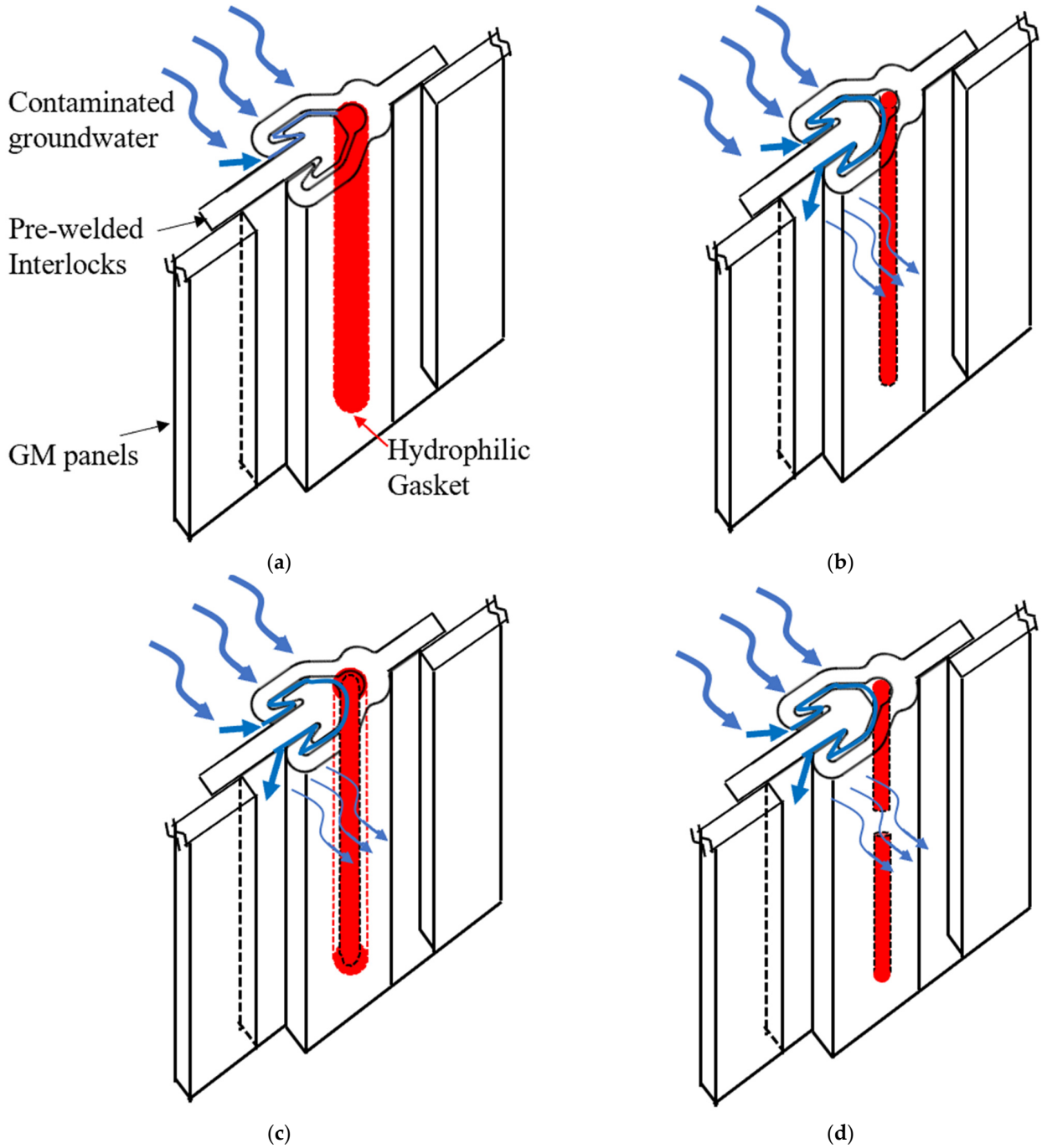

Figure 1. Schematics of the effect of contaminants on swelling ratio and leakage of the hydrophilic gaskets: (**a**) the high swelling ratio of the gasket with an intact seal, (**b**) the low swelling ratio of the gasket, (**c**) the high swelling ratio of the gasket with expansion-relaxation, and (**d**) defective Hydrophilic gasket with fracture.

To sum up, the significant challenges of the composite geomembrane vertical cutoff walls used in contaminated sites included the defects of the hydrophilic gasket during installation, the swelling capacity of that immersed in contaminated liquids, and the relaxation characteristics after expansion. Thus, in this paper, several laboratory tests were conducted to investigate the prolonged swelling behavior, relaxation characteristics

after expansion, flow rates, self-healing of the hydrophilic gasket under contaminants soaking or permeation, and micro-morphology of hydrophilic gasket under complex contaminated conditions.

This study aimed to evaluate the prolonged swelling performance, flow rates, self-healing of hydrophilic gaskets soaked in the deionized water (DIW), MSW landfill leachates, NaCl solutions, and $CaCl_2$ solutions of different concentrations through laboratory tests. To explore the swelling behavior and relaxation properties after expansion, swelling tests were conducted, and the swelling ratios (radial swelling ratio, free swelling ratio of weight, and volume) of hydrophilic gaskets were determined. A flow rates test apparatus (modified from [15,37–39]) was manufactured to evaluate the flow rates and self-healing characteristic of the hydrophilic gasket with contaminated liquids permeation. Based on the scanning electronic microscope (SEM), the micro-morphology of the hydrophilic gasket was investigated. The findings are anticipated to be insightful in determining the impact of salt solutions and MSW landfill leachates on the prolonged swelling performance and flow rates of hydrophilic gaskets.

2. Materials and Methods

2.1. Materials

The materials prepared in this paper consisted of the hydrophilic gasket, interlocks pre-welded in the geomembrane panel, testing solutions, and backfill sand. The commercial hydrophilic gasket tested in this study was manufactured by Hairui Engineering Rubber Co., Ltd. (Hengshui, China). The components and quantities of the raw materials for the hydrophilic gasket used in this study were shown in Table 1. The ingredients included chlorinated polyethylene (CPE), sodium polyacrylate (PAAS), chlorinated paraffin, dicumyl peroxide, palmitic acid, stearic acid, SiO_2, and color agent. The HDPE geomembrane, which thickness is 3 mm, was obtained from Atarfil (Granada, Spain). The interlock was manufactured and pre-welded with geomembranes by Jiangsu Shengtai Environmental Technology Co., Ltd. (Nanjing, China). The hydraulic conductivity of the geomembrane with pre-welded interlock is 1.5×10^{-12} m/s. The sand was sourced from the Yangzi River floodplains in Nanjing, China. It was cleaned with deionized water, air-dried, and sieved using a No.18 (1-mm) mesh in accordance with ASTM D698 [40]. According to the ASTM D2487 Unified Soil Classification System (USCS) [41], the sand had a curvature coefficient and uniformity coefficient of 3.66 and 0.76, respectively, suggesting that it was poorly graded.

Table 1. Compositions of the hydrophilic gasket used in this study.

Title 1 Chemical	Mass Content (%)
Chlorinated polyethylene (CPE)	42.5
SiO_2	17
Chlorinated paraffin	12
Sodium polyacrylate (PAAS)	12
Palmitic acid	8.5
Stearic acid	4.5
Dicumyl peroxide (DCP)	2.5
Color agent	1

2.2. Testing Liquids

The testing liquids used in this study were deionized water (DIW), MSW landfill leachates, NaCl solutions, and $CaCl_2$ solutions prepared using DIW. The MSW landfill leachates were obtained from the MSW landfill located in Wenzhou, China. Table 2 lists the chemical characteristics of the MSW landfill leachates. Equations (1) and (2) were used to calculate the ionic strength (I), and relative abundance of monovalent and multivalent cations (RMD) [42], as follows:

$$I = \frac{1}{2} \sum C_j Z_j^2 \quad (1)$$

where C_j and Z_j are the molar concentration (mM) and the principal charge of cation species j, respectively.

$$RMD = M_M / M_D^{0.5} \quad (2)$$

where M_M is the total molarity of monovalent cations in the solution, and M_D is the total molarity of multivalent cations in the solution.

Table 2. Chemical properties of the MSW landfill leachate used in this study.

Property	Details
Sodium (mg/L)	860
Calcium (mg/L)	128
Magnesium (mg/L)	39.3
Iron (mg/L)	6.62
Aluminum (mg/L)	2.16
Copper (mg/L)	0.0247
Nickel (mg/L)	0.486
Zinc (mg/L)	0.246
Cadmium (mg/L)	0.00016
Manganese (mg/L)	0.0207
Chromium (mg/L)	5.77
Lead (mg/L)	0.0162
Arsenic (mg/L)	0.104
Sulfate (mg/L)	254
Ammonia nitrogen (mg/L)	2160
Total nitrogen, TN (mg/L)	2240
Total phosphorus, TP (mg/L)	28.5
Chemical Oxygen Demand (COD_{cr}), (mg/L)	5450
Biological Oxygen Demand (BOD_5), (mg/L)	1400.3
Ionic strength, I (mM)	63.18
RMD ($mM^{1/2}$)	9.01

Combining a given quantity of NaCl and $CaCl_2$ powder (Analytical Reagent, Sinopharm Chemical Reagent Co., Ltd., Shanghai, China) with a predetermined volume of DIW, different starting concentrations (c_0) of the NaCl and $CaCl_2$ solutions were prepared. The c_0 values were 10, 20, 50, and 100 mM. A pH/EC meter (Thermo Fisher Scientific Company, MA, USA) was used to measure each produced testing liquid's pH and electrical conductivity (EC) in accordance with ASTM E70 [43] and ASTM D1125 [44], respectively. Each testing liquid had its pH and EC measured in triplicate samples, and the average results were calculated. The average values of these fundamental chemical characteristics of testing liquids were listed in Table 3.

Table 3. The average values of these fundamental chemical characteristics of testing liquids.

Testing Liquids	Target Concentration (mM)	Measured Concentration (mM)	*EC* at 25 °C (mS/cm)	pH	Ionic Strength, *I* (mM)
DIW	N/A	N/A	0.00134	6.91	0
NaCl solution	10	10.10	1.228	7.03	5.05
	20	19.95	2.35	6.9	9.98
	50	50.12	5.72	6.67	25.06
	100	99.95	10.73	6.54	49.98
$CaCl_2$ solution	10	9.90	2.28	7.72	19.8
	20	20.10	4.3	7.43	40.2
	50	50.10	9.9	7.19	100.2
	100	100.10	18.94	7.02	200.2
MSW landfill leachates	N/A	N/A	35.4	8.48	63.18

2.3. Testing Meathods and Apparatus

2.3.1. Swelling Tests

To explore the swelling behavior and relaxation characteristics of the specimens immersed in DIW, MSW landfill leachates, NaCl solutions, and CaCl2 solutions, the free swelling ratio (of weight S_w and volume S_v) and radial swelling ratio (S_a) were chosen as parameters. Throughout all trials, the room temperature was kept at 25 ± 1 °C, and the relative humidity was kept at 64% ± 2%.

1. Free swelling tests.

Free swelling tests were conducted, and the S_w and S_v values of the specimens were established to investigate the impacts of contaminated groundwater on the swelling behavior of the samples. The detailed test procedures were as follows: first, the specimens were cut into cylinders with a diameter of 6 mm and a length of 20 mm. The number of parallel specimens was three. Next, the original weight and volume of the specimens were determined using an electronic balance with a 0.001 g accuracy, and a Vernier caliper with a 0.01 mm accuracy. Then, the triple specimens were placed in a sealed container, and 200 mL testing liquids, including the DIW, MSW landfill leachates, NaCl solutions with concentrations of 10, 20, 50, 100 mM, and $CaCl_2$ solutions with concentrations of 10, 20, 50, 100 mM, were added, respectively. Finally, the specimens were taken out of the container using a tweezer at a precise time. Their surfaces were cleaned with tissue paper in preparation for weighing and volume testing. These procedures repeated until they reached equilibrium states. The S_w and S_v were calculated as per ASTM 3616-2014 [45], as Equations (3) and (4).

$$S_w = \frac{W_t - W_0}{W_0} \times 100\% \quad (3)$$

where W_0 represents the specimen's initial weight, and W_t represents the weight after swelling at time t. S_w is the swelling ratio of weight.

$$S_v = \frac{V_t - V_0}{V_0} \times 100\% \quad (4)$$

where V_0 represents the specimen's initial volume, and V_t represents the volume after swelling at time t. S_v is the swelling ratio of volume.

2. Radial swelling tests.

The radial swelling tests were conducted to investigate the relaxation characteristics of the hydrophilic gasket. To ensure the reliability of the test results, specimens were strictly cut into a cylinder with a diameter of 6 mm and a length of 20 mm. The testing apparatus (see Figure 2) used in this experiment was modified from a WG triplex low-pressure single lever consolidation instrument (Nanjing Soil Instrument Factory Co., Ltd., Nanjing, China), which consisted of three parts: a compression device, a corrosion resistance device, and a dial gauge. The test was conducted as follows: first, the four specimens were horizontally positioned to ensure the balance during swelling in the corrosion-resistant device. The device was consisted of a corrosion-resistance container (150 mm in diameter and 100 mm in height), a porous stone (70 mm in diameter, 8 mm in height diameter of 70 mm, and height of 8 mm) at the bottom of the container, a corrosion-resistance ring (61.88 mm in diameter and 50 mm in height) at the top of porous stone, and a corrosion-resistance cap (61 mm in diameter) at the top of the specimens. The specimens were subjected to a vertical force using a loading apparatus to imitate the expansion pressure between a hydrophilic gasket and interlocks. Weights of 3.836 kg were applied to the hydrophilic gasket. Finally, 1000 mL testing liquids, including the DIW, MSW landfill leachates, NaCl solutions (100 mM), and $CaCl_2$ solutions (100 mM), were gradually added into the corrosion-resistance containers, respectively. The dial gauge captured the vertical displacements at various time-steps while

the specimens swelled in the testing solutions. The radial swelling ratio (S_a) is defined as follows:

$$S_a = \frac{\Delta}{D} \times 100\% \quad (5)$$

where Δ represents the radial displacement variation of the specimen, and D is the original diameter of the specimen (6 mm).

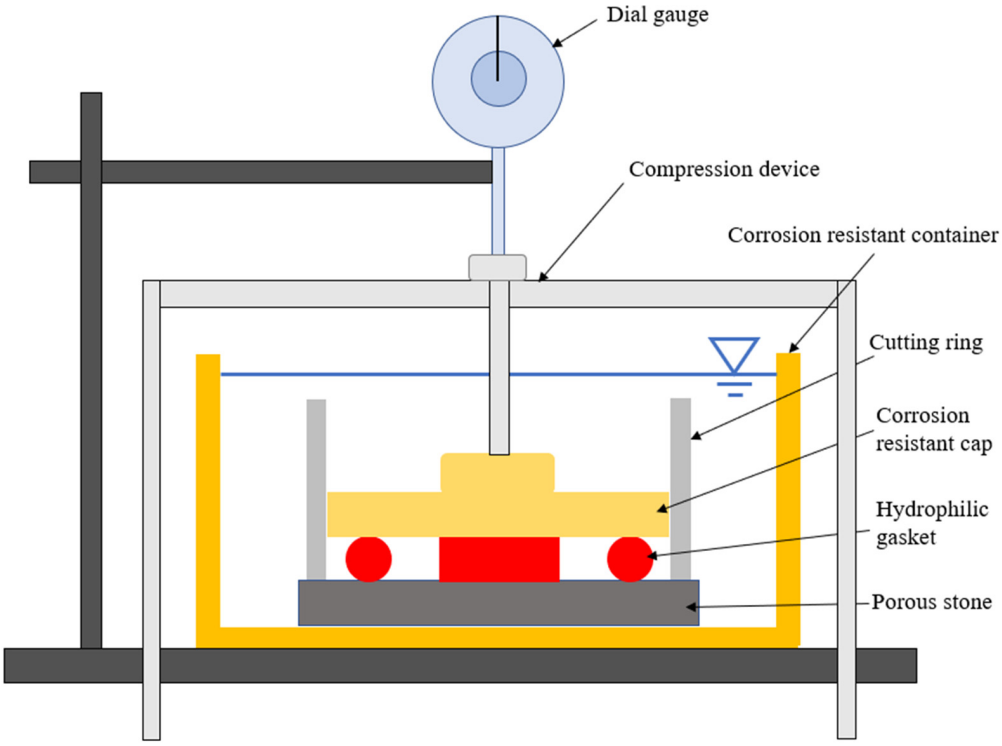

Figure 2. The schematic of radial swelling test devices modified from a single lever consolidation instrument.

2.3.2. Flow Rates Model Tests and Apparatus

The testing apparatus used in the model test was schematically presented in Figure 3a,b. The flow rates testing apparatus consisted of the following components with different functions and materials: (1) baseboard with the component of Teflon; (2) lower model chamber manufactured with the corrosion-resistant steel with a diameter of 250 mm and a height of 100 mm; (3) splint with the component of Teflon for the immobilization and sealing of geomembranes; (4) upper model chamber manufactured with organic glasses with a diameter of 250 mm and a height of 100 mm; (5) sealing cover plate with the component of Teflon; (6) upper barrier materials; (7) lower barrier materials; (8) the lower perforated plate with the component of Teflon, which porosity is 85%; (9) the upper perforated plate with the component of Teflon, which porosity is 85%; (10) pressure transducer (VWE-0.4Q, Nanjing Genan Industrial Co., Ltd., Nanjing, China) had an 0–400 kPa pressure range with the accuracy of 0.1 kPa; (11) A data acquisition system (MCU-32, Nanjing Genan Industrial Co., Ltd., Nanjing, China) was capable of simultaneously collecting data for up to 32 channels; (12) geomembranes with the pre-welded interlocks; (13) bolts; (14) vinyl tubing with bidirectional valves; (15) a measuring cylinder; (16) a piezometer; (17) bidirectional valves; (18) a reservoir with the component of Teflon; (19) the air pressure controller; (20) the air compressor; (21) the seal ring with the component of Teflon; (22) the heightening plate with a height of 50 mm; (23) the sketch plate; (24) the lower side wall; and (25) the upper side wall.

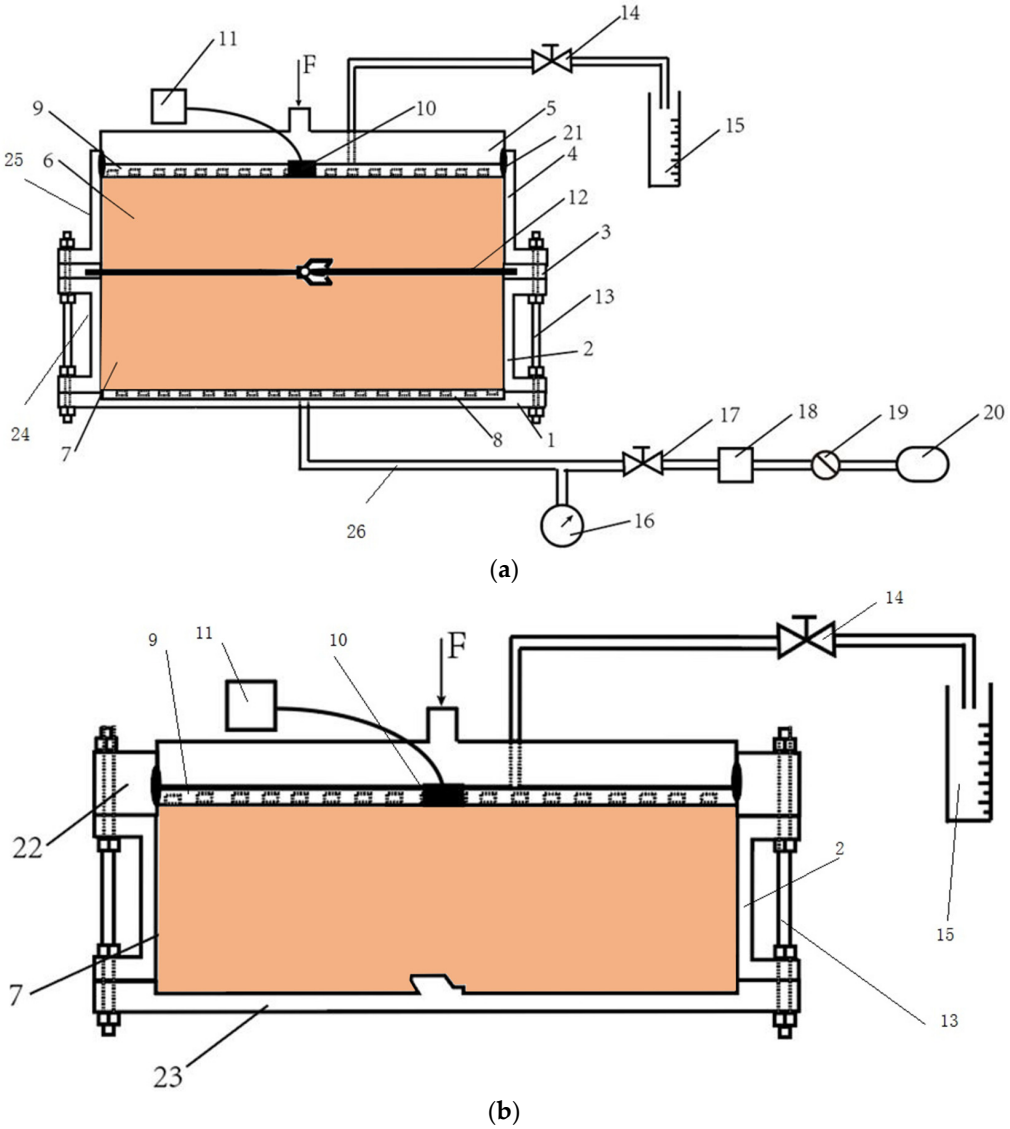

Figure 3. The schematic of (**a**) a flow rates model testing apparatus, and (**b**) a consolidation model testing device used in this study.

The experiments using the flow rates model apparatus were completed as per the following steps: first, the consolidation model device was assembled as Figure 3b. Then, the sand was placed into the chamber, which had a slump height of 125 mm per ASTM C143 [46] and was saturated with DIW. Second, the upper perforated plate and cover plate were installed for good sealing with the pressure transducer in contact with the top of the sand. The consolidation of the sand was conducted through the loading of the cover plate. It was completed when the volume of liquid in the measuring cylinder stayed the same. Then, the lower model chamber with compressed sand was inverted, and the heightening plate and sketch plate were detached. Next, the apparatus was assembled as Figure 3a, and the poor-sealing specimens with a fracture width of 10 mm were installed in the interlocks like in Figure 4a. The consolidation of sand in the upper chamber was the same as the aforementioned procedure. Finally, the testing liquid was added to the reservoir, and the penetration test was conducted with a hydraulic gradient (*i*) of 20 and a confining pressure of 50 kPa. The liquid volume and elapsed time were recorded and the flow rates were calculated by Equation (6).

$$Q = \frac{\Delta V}{\Delta t} \ / \ \mathrm{L} \tag{6}$$

where Q is the flow rates, unit mL/s/m; $\frac{\Delta V}{\Delta t}$ represents the flow rates during Δt with the elapsed time, unit mL/s, and L is the length of the interlocks (0.25 m).

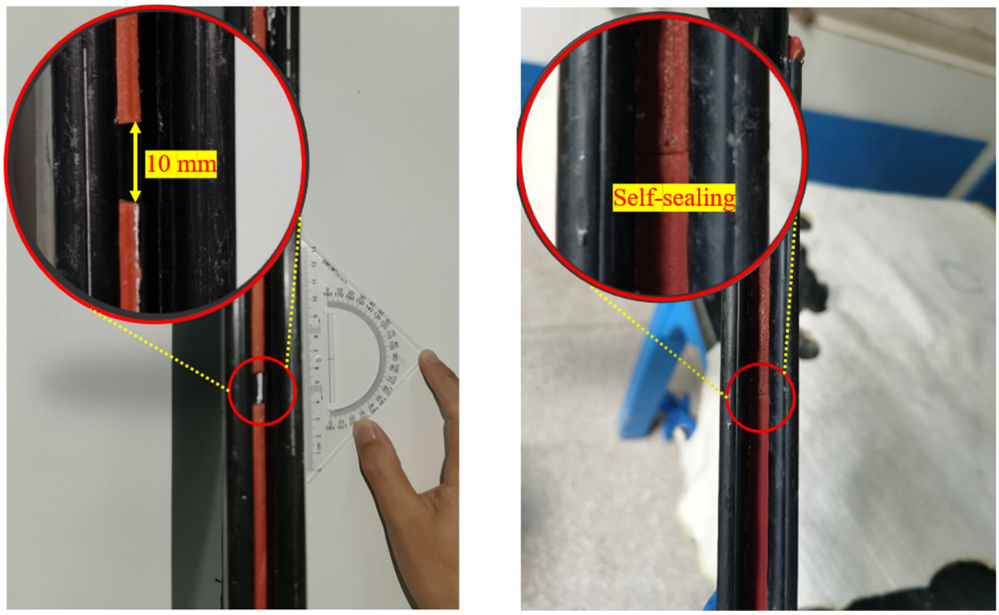

(**a**) (**b**)

Figure 4. The pictures of: (**a**) installation of poor-sealing hydrophilic gaskets before testing, and (**b**) the self-healing behavior of the specimen after the DIW penetration.

2.3.3. Scanning Electron Microscope (SEM) Tests

Image analyses using SEM (SU3500, Hitachi High-Tech, Tokyo, Japan) were conducted on the specimens before and after soaked in the DIW, MSW landfill leachates, NaCl solutions (100 mM), and $CaCl_2$ solutions (100 mM) to evaluate microstructure changes. First, the specimens obtained from the prolonged free swelling tests were cut into 1 cm^3 piece. The SEM samples were frozen in liquid nitrogen for five minutes at −120 °C. Moisture was sublimated at −80°C for 24 hours at a vacuum freeze-drying unit pressure of −18 N. (Nanjing Xianou Instruments Manufacture Co., Ltd., Nanjing, China). The frozen SEM specimens were freeze-dried, cut into small blocks with a natural fracture surface area of roughly 0.25 cm^2, coated with a thin layer of gold, then subjected to SEM examinations. For the SEM testing, three specimens were tested, and a representative image was chosen.

3. Results and Discussion

3.1. Free Swelling Tests Results

The effects of the DIW, NaCl solutions, $CaCl_2$ solutions, and MSW landfill leachates on the free swelling behavior (S_w and S_v) of hydrophilic gaskets are shown in Figure 5. Basically, the S_w and S_v increased with the passage of time. However, the S_w and S_v curves of $CaCl_2$ solutions with different concentrations presented a rising tendency in the early stages (0–40 days), and the S_w and S_v of the specimens decreased almost 25–50% after reaching their peak values (Figure 5c). The precipitation and shedding of components under strong multivalent ionic conditions were also possible explanations for this phenomenon. According to Figure 5a, the specimens that submerged in the DIW had the greatest capacity to absorb water, with a S_w of 2145% and S_v of 2465%. It was attributed to the swelling mechanisms of the SAP and hydrophilic gaskets. Water molecules permeated into the PAAS via capillary action and diffusion when the hydrophilic gasket contacted with the water [22,47]. The negative ion (COO-) became fixed to the PAAS chain, and the cation became detachable as the ionization group (Na+) of the PAAS chain was ionized in the water. Consequently, the detachable cation altered the concentration of the internal and external solutions, the chain extended due to electrostatic forces, and the water kept entering the

PAAS. Following chain extension, electrostatic forces gradually diminished, and more water was added, causing the concentration difference between the internal and external solutions diminish gradually. Suction balance was eventually attained as the electrostatic forces gradually vanish [17,21,48–50]. Figure 5b,c showed that the S_w and S_v tended to decrease with the increase in the ion concentration gradient. Due to the amount of water absorbed by the PAAS, which decreased with the increase in concentration of the external solution [18,48,51,52]. The S_w of specimens soaked in NaCl solutions with concentrations of 10, 20, 50, and 100 mM was 1208, 926, 605, and 428%, respectively, and the S_v was 1579, 1204, 737, and 529%, respectively. Figure 5d showed that the S_w and S_v of specimens soaked in the leachates were higher than those of $CaCl_2$ solutions, which the S_w was 240% and the S_v was 313%, respectively. Moreover, the S_w and S_v of specimens soaked in the leachates were lower than those of all NaCl solutions and far less than those of DIW. It could be inferred that the multivalent ions considerably influenced the free swelling behavior of hydrophilic gaskets [48]. The curves showed that the trend of the S_w was similar to that of S_v. Since the weight of the specimens could be measured more easily and quickly than the volume, the S_w could be used as an indicator of free swelling behavior.

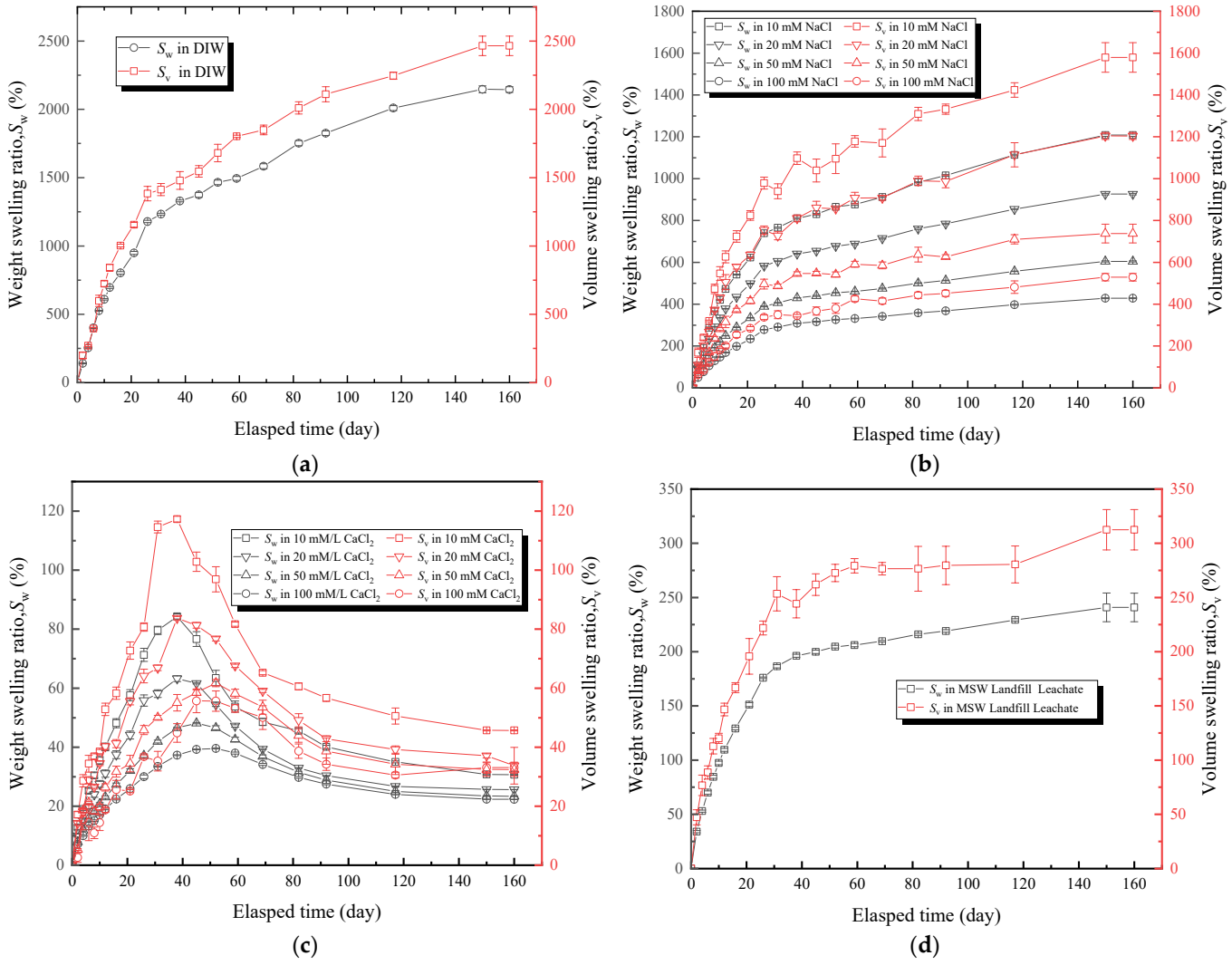

Figure 5. The effect of testing liquids: (**a**) the DIW, (**b**) NaCl solutions with different concentrations, (**c**) $CaCl_2$ solutions with different concentrations, and (**d**) MSW landfill leachates on free swelling ratio (S_w and S_v) of specimens.

3.2. Radial Swelling Tests Results

The results of radial swelling ratio with an elapsed time of specimens immersed in the DIW, NaCl solutions (100 mM), $CaCl_2$ solutions (100 mM), and MSW landfill leachates were shown in Figure 6. In general, the S_a of all specimens increased with the elapsed time and reached its peak after 30–50 days of loading. Then, the S_a decreased significantly, which was the relaxation phenomenon. The relaxation became more distinct when the specimens was soaked in the DIW, in which the S_a was 56% at peak and 25% in a stable state. That relaxation ratio (defined as dividing the difference between the S_a at peak and in a stable state into the S_a at peak) was 55%. For specimens tested in NaCl solutions (100 mM), $CaCl_2$ solutions (100 mM), and MSW landfill leachates, the S_a was 29.8, 9.2, and 22.3% at peak and 16, 3.3, and 10.7% in a stable state, and the relaxation ratio was 46, 64, and 52%, respectively. This phenomenon could be explained from three aspects. First, under loading pressure, the chain of PAAS and matrix could not expand sufficiently, causing the hydrophilic gasket to absorb less water [48]. Second, the insufficiently expanded PAAS separated from the matrix after reaching the peak of expansion due to the poor compatibility of the matrix with PAAS [18,26,28]. Third, the swelling ability of hydrophilic gaskets could not be kept constant with time under constant loading pressure [17,35,36].

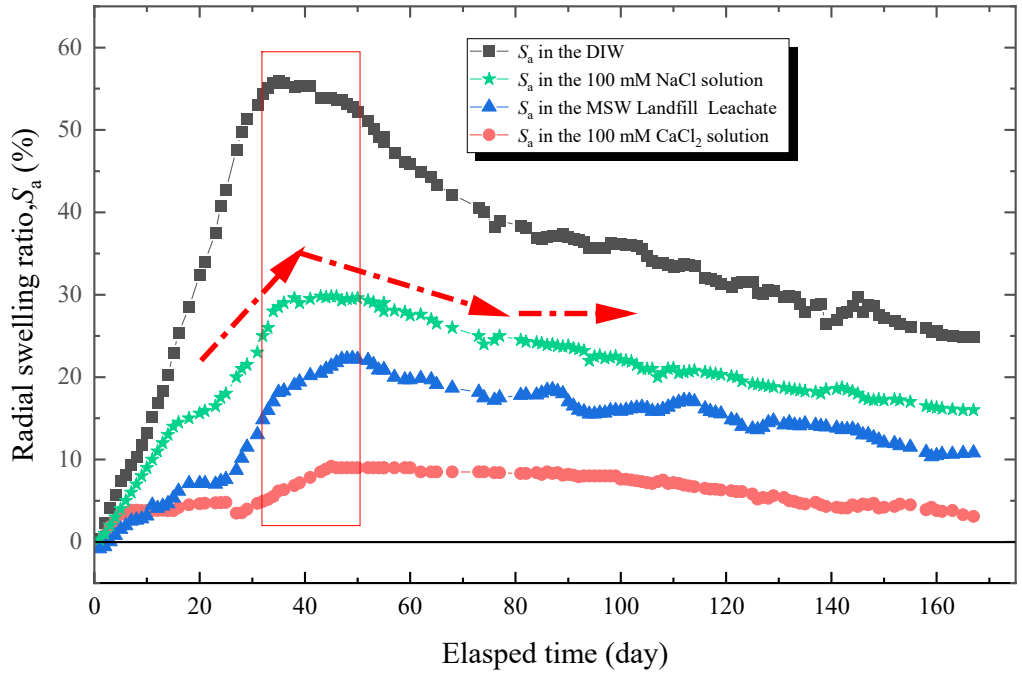

Figure 6. The radial swelling test results of specimens with different testing liquids.

3.3. Flow Rates Tests Results

The flow rates with an elapsed time of poor-sealing specimens (see Figure 4a), which penetration with the DIW, NaCl solutions (100 mM), $CaCl_2$ solutions (100 mM) were shown in Figure 7. The results showed that the specimen penetrated with the DIW had the lowest flow rates, followed by NaCl and $CaCl_2$ solutions, regardless of the elapsed time. For specimens penetrated with the DIW, the flow rates decreased sharply at the first 10 days, then decreased slowly to zero at day 42, and finally increased gradually after day 51, when the flow rates were 0.099 mL/s/m in a stable state. This phenomenon is because the PAAS had the best absorption capacity when contacted with the DIW and swelled rapidly at the initial stage. Then, the swelling ratio increased, and flow rates decreased slowly because the swelling of the specimen was confined by interlocks, and the contact pressure increased slowly [17–19]. Finally, the flow rates reached zero when the contact pressure was higher than the penetration pressure. However, the flow rates increased again at a plodding speed because of the relaxation of the hydrophilic gasket. The causes were

similar to those aforementioned, the contact pressure was not constant, and decreased after relaxation. Then, the degree of relaxation was lower than the specimens in radial swelling tests. Therefore, the increasing speed of flow rates was extremely slow before reaching a stable state. Moreover, the self-healing of the material could be observed in Figure 4b. Due to the hydrophilic gasket could swell along the axial direction when it confined along radial direction. For specimens penetrated with NaCl and $CaCl_2$ solutions with a concentration of 100 mM, the trend of the curves was basically the same. For specimens penetrated with NaCl solutions, the flow rates decreased sharply at first (23 days), then decreased slowly during days 23–33, and decreased sharply to zero at day 48, finally increasing gradually to a stable state (0.399 mL/s/m). Additionally, the flow rates of specimens penetrated with $CaCl_2$ solutions decreased to 0.855 mL/s/m at day 59, then increased slowly to a stable state (1.148 mL/s/m). The difference was that the flow rates of specimens penetrated with NaCl solution were much lower than those of $CaCl_2$ solutions. The relationship between the flow rates of the poor-sealing hydrophilic gaskets and the S_w, S_v, S_a, and type of liquids was shown in Figure 8. There were two causes for the results: first, the ionic strength of a 100 mM NaCl solution was lower than that of $CaCl_2$. Second, the impact of the total of monovalent multivalent cations in the solution on swelling behavior and the flow rates were more significant than that of molarity cations.

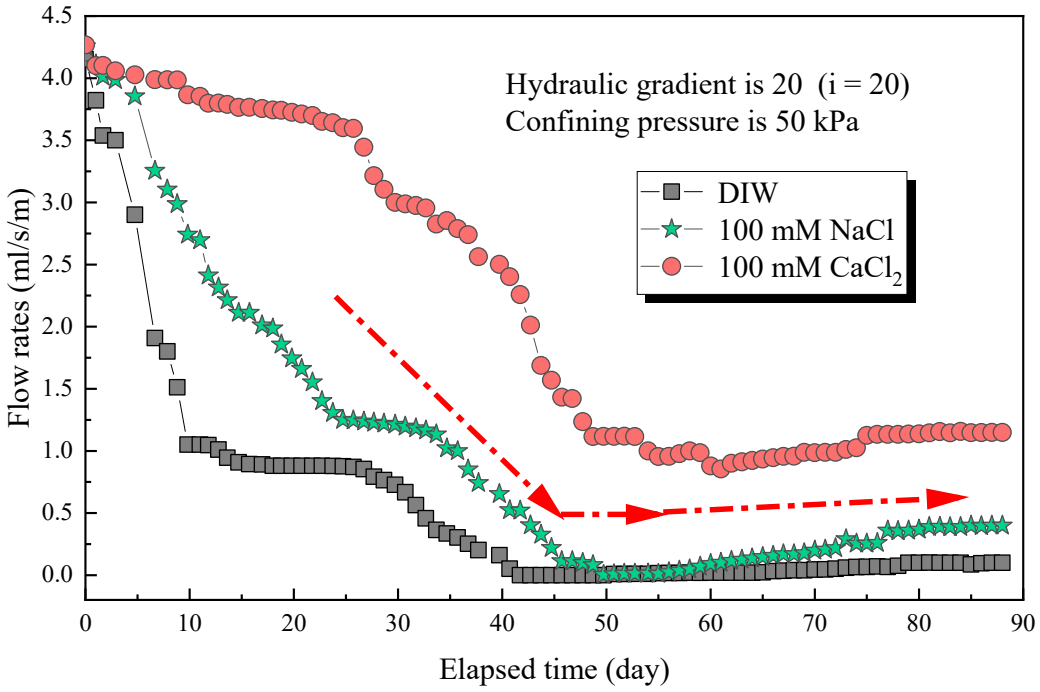

Figure 7. The flow rates with elapsed time of poor-sealing specimens permeated with different testing liquids.

3.4. Scanning Electron Microscope (SEM) Tests Results

This section evaluated the microdamage and morphology of the hydrophilic gasket following submersion in the DIW, NaCl solutions (100 mM), $CaCl_2$ solutions (100 mM), and MSW landfill leachates. Figure 9 presented the SEM images for specimens immersed in different testing liquids. Figure 9a presented the SEM image of the original specimen. The original surface of the specimen had a few thin cracks and contained some additives and SAP (sodium polyacrylate). The thin crack formed could have been caused by some SAP materials being incompatible with the CPE matrix during the production mixing procedure [18,19]. Figure 9b presented the SEM images of the specimen immersed in the DIW. There were many long-chain sodium polyacrylate (PAAS) absorbing enough water that the matrix structure was propped up by the swelling PAAS. Therefore, the specimens could swell up to 2400%, as shown in Figure 5a. The SEM images of the specimen soaked in

the NaCl solution with a concentration of 100 mM were shown in Figure 9c. The PAAS was not swelling enough because the ionization group on the chain was difficult to ionize in the water because of the high concentration of Na^+ in the solution. Thus, the SAP network could not expand because of the low electrostatic repulsion between the negative ions in the chain [17,21]. Moreover, several small cavities with a diameter of 1–3 μm appeared in the specimen due to the PAAS separating from the specimen during the water-absorbing process [28]. Figure 9d presented the SEM images of the specimen after immersion in the $CaCl_2$ solution with a concentration of 100 mM. There were numerous large cracks with a length of 5–12 μm, and a little PAAS expanding very little on the surface of the specimen. This phenomenon was attributed to numerous long-chain expanding PAAS separating from the matrix due to the high ionic strength of the $CaCl_2$ solution. Finally, the SEM image of the specimen after soaked in MSW landfill leachates was shown in Figure 9e. In the picture, cavities with a diameter of 5 μm and shallow cracks with a length of 6 μm could be observed. It was attributed to the PAAS separating from the matrix during swelling. The micro-morphology above indicated that the SAP with insufficient expansion could separate from the matrix under the high multivalent ionic strength or loading pressure conditions.

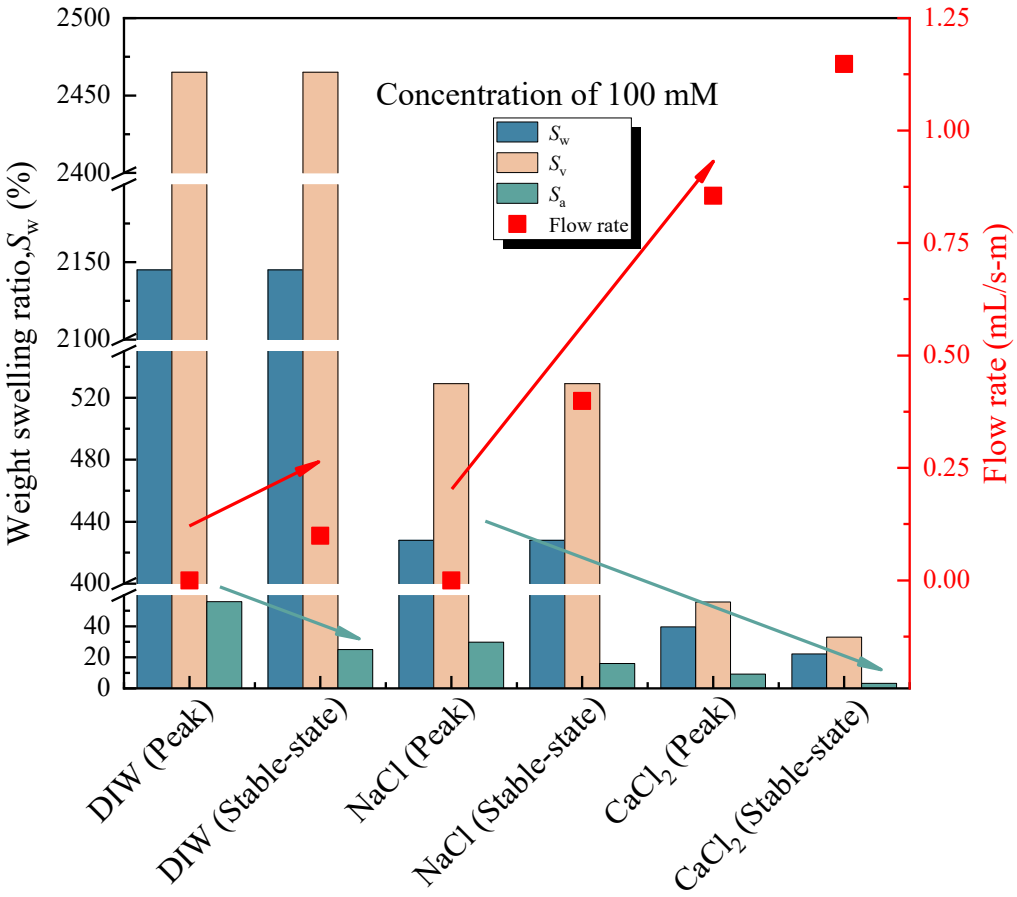

Figure 8. The relationship between the flow rates of the poor-sealing hydrophilic gaskets and the S_w, S_v, S_a, and type of liquids.

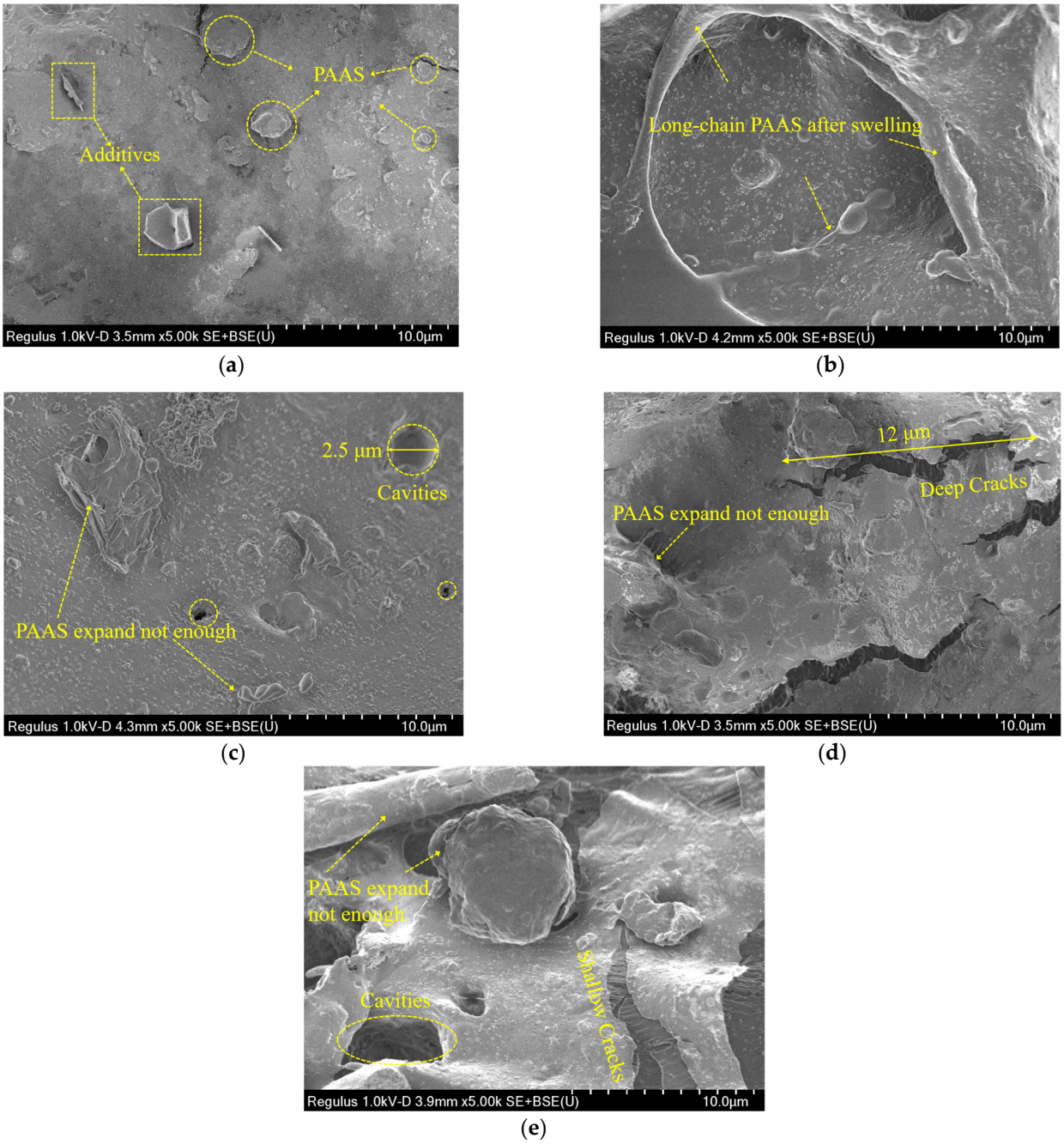

Figure 9. The SEM images of specimens immersed in: (**a**) original specimen, (**b**) the DIW, (**c**) the NaCl solution (100 mM), (**d**) the $CaCl_2$ solution (100 mM), and (**e**) MSW landfill leachates.

4. Conclusions

The free swelling ratio of the hydrophilic gaskets exposed to the DIW, MSW landfill leachates, NaCl solutions, and $CaCl_2$ solutions with different concentrations was investigated. The radial swelling ratio and relaxation characteristics were also investigated using a device modified from single lever consolidation instrument. A flow rates model apparatus was manufactured and employed to measure the flow rates of the poor-sealing hydrophilic gasket. Finally, the SEM was performed to investigate the micro-damage morphology of the hydrophilic gaskets. The following conclusions can be drawn in light of the results.

- The S_w and S_v of the hydrophilic gasket material soaked in the DIW were the highest, followed by NaCl solutions, MSW landfill leachates, and $CaCl_2$ solutions. The S_w and S_v curves of specimens immersed in $CaCl_2$ solutions increased in the initial stage,

then decreased until a stable state. The results illustrated that the ionic strength and multivalent cations greatly impacted the swelling behavior of hydrophilic gaskets.

- For specimens tested in the DIW, the NaCl solution (100 mM), the $CaCl_2$ solution (100 mM), and MSW landfill leachates, the S_a was 56, 29.8, 9.2, 22.3% at peak and 25, 16, 3.3, 10.7% in a stable state, and the relaxation ratio was 55, 46, 64, 52%, respectively.
- The self-healing of the hydrophilic gasket was observed. The flow rates of specimens penetrated with DIW, NaCl, and $CaCl_2$ decreased to a stable state, which was 0, 0, 0.855 mL/s/m, respectively, then increased extremely slowly to the stable values of 0.099, 0.399, and 1.148 mL/s/m, respectively. The flow rates of the hydrophilic gasket penetrated with the DIW were the lowest, followed by the NaCl solution (100 mM), and the $CaCl_2$ solution (100 mM), which was attributed to the effect of the multivalent ionic strength on the swelling capacity of the hydrophilic gasket.
- The SEM images showed that there was a lot of long-chain expanded PAAS, the matrix immersed in DIW could be propped up and expanded to a large volume. However, there were numerous microcracks or microcavities on the surface of specimens immersed in the $CaCl_2$ solution (100 mM) and the MSW landfill leachates. This explained the results of the difference of the free swelling ratio of hydrophilic gaskets immersed in different solutions. The micro-morphology indicated that the SAP with insufficient expansion could separate from the matrix under the high multivalent ionic strength.

Author Contributions: Conceptualization, M.W., X.F. and Y.D.; methodology, M.W., Y.D. and X.F.; software, M.W.; validation, M.W. and N.J.; formal analysis, M.W. and Z.J.; investigation, M.W., C.C. and Z.J.; resources, M.W.; data curation, M.W. and Z.J.; writing—original draft preparation, M.W., X.F., C.C. and N.J.; writing—review and editing, M.W., Y.D., X.F. and N.J.; visualization, M.W.; supervision, M.W., Y.D. and X.F.; project administration, Y.D.; funding acquisition, Y.D. All authors have read and agreed to the published version of the manuscript.

Funding: Financial support for this project was provided by the National Key R&D Program of China (Grant No. 2018YFC1803100 and 2018YFC1802300), the National Natural Science Foundation of China (Grant Nos. 41877248, and 42177133).

Data Availability Statement: Some or all data, models, or code that support the findings of this study are available from the corresponding author upon reasonable request.

Conflicts of Interest: The authors declare no conflict of interest.

References

1. Fu, X.L.; Shen, S.Q.; Reddy, K.R.; Yang, Y.L.; Du, Y.J. Hydraulic conductivity of sand/biopolymer-amended bentonite backfills in vertical cutoff walls permeated with lead solutions. *J. Geotech. Geoenviron. Eng.* **2022**, *148*, 04021186. [CrossRef]
2. Fu, X.L.; Zhang, R.; Reddy, K.R.; Li, Y.C.; Yang, Y.L.; Du, Y.J. Membrane behavior and diffusion properties of sand/SHMP-amended bentonite vertical cutoff wall backfill exposed to lead contamination. *Eng. Geol.* **2021**, *284*, 106037. [CrossRef]
3. Du, Y.J.; Fan, R.D.; Liu, S.Y.; Reddy, K.R.; Jin, F. Workability, compressibility and hydraulic conductivity of zeolite-amended clayey soil/calcium-bentonite backfills for slurry-trench cutoff walls. *Eng. Geol.* **2015**, *195*, 258–268. [CrossRef]
4. Du, Y.J.; Fan, R.D.; Reddy, K.R.; Liu, S.Y.; Yang, Y.L. Impacts of presence of lead contamination in clayey soil–calcium bentonite cutoff wall backfills. *Appl. Clay Sci.* **2015**, *108*, 111–122. [CrossRef]
5. Lee, T.; Benson, C.H. Flow past bench-scale vertical ground-water cutoff walls. *J. Geotech. Geoenviron. Eng.* **2000**, *126*, 511–520. [CrossRef]
6. Peng, C.H.; Feng, S.J.; Chen, H.X.; Ding, X.H. An analytical model for one-dimensional diffusion of degradable contaminant through a composite geomembrane cut-off wall. *J. Contam. Hydrol.* **2021**, *242*, 103845. [CrossRef]
7. Thomas, R.W.; Koerner, R.M. Advances in HDPE barrier walls. Geotext. *Geomembranes* **1996**, *14*, 393–408. [CrossRef]
8. Liu, L.; Liu, Y.; Zhen, S.; Ding, S.; Jin, J.; Wang, Y.; Ge, Y. Applications of Geomembrane Cutoff Walls in Remediation of Contaminated Sites. In Proceedings of the 8th International Congress on Environmental Geotechnics Volume 2: Towards a Sustainable Geoenvironment, Singapore, 11 October 2018; Springer: Berlin/Heidelberg, Germany, 2018; p. 335.
9. Kavazanjian, E., Jr.; Dixon, N.; Katsumi, T.; Kortegast, A.; Legg, P.; Zanzinger, H. Geosynthetic barriers for environmental protection at landfills. In Proceedings of the Geosynthetics-8th International Conference on Geosynthetics, Yokohama, Japan, 18–22 September 2006; pp. 121–152.

10. Peng, C.H.; Feng, S.J.; Zheng, Q.T.; Ding, X.H.; Chen, Z.L.; Chen, H.X. A two-dimensional analytical solution for organic contaminant diffusion through a composite geomembrane cut-off wall and an aquifer. *Comput. Geotech.* **2020**, *119*, 103361. [CrossRef]
11. Tachavises, C.; Benson, C.H. Hydraulic Importance of Defects in Vertical Groundwater Cut-Off Walls. In Proceedings of the In Situ Remediation of the Geoenvironment, Minneapolis, MN, USA, 5–8 October 1997; Evans, J.C., Ed.; American Society of Civil Engineers: Reston, VA, USA, 1997; pp. 168–180.
12. Qian, X.; Zheng, Z.; Guo, Z.; Qi, C.; Liu, L.; Liu, Y.; Ge, Y. Applications of geomembrane cutoff walls in remediation of contaminated sites. In *The International Congress on Environmental Geotechnics*; Springer: Singapore, 2018; pp. 335–342.
13. Koerner, R.M.; Guglielmetti, J.L. Vertical barriers: Geomembranes, assessment of barrier containment technologies, a comprehensive treatment for environmental remediation applications. In Proceedings of the International Containment Technology Workshop, Baltimore, MD, USA, 29–31 August 1995; Rumer, R.R., Mitchell, J.K., Eds.; pp. 95–118.
14. Zhen, S.; Huo, C.; He, Z.; Zheng, Z.; Zheng, F.; Sun, X.; Liu, L. Application and comparative study of vertical barrier technology. *Environ. Sanit. Eng.* **2017**, *25*, 51–56.
15. Bouazza, A.; Zornberg, J.G.; Adam, D. Geosynthetics in Waste Containment Facilities: Recent Advances. State-of-the-Art keynote paper. In Proceedings of the Seventh International Conference on Geosynthetics, Nice, France, 22–27 September 2002; Balkema, A.A., Ed.; Volume 2, pp. 445–510.
16. Daniel, D.E.; Koerner, R.M. On the use of geomembranes in vertical barriers. In Proceedings of the Advances in Transportation and Geoenvironmental Systems Using Geosynthetics, Denver, CO, USA, 5–8 August 2000; pp. 81–93.
17. Yang, C.; Shen, S.L.; Hou, D.W.; Liao, S.M.; Yuan, D.J. Material properties of the seal gasket for shield tunnels: A review. *Constr. Build. Mater.* **2018**, *191*, 877–890. [CrossRef]
18. Dehbari, N.; Tang, Y. Water swellable rubber composites: An update review from preparation to properties. *J. Appl. Polym. Sci.* **2015**, *132*, 42786. [CrossRef]
19. Wang, G.; Li, M.; Chen, X. Preparation and water-absorbent properties of a water-swellable rubber. *J. Appl. Polym. Sci.* **1998**, *68*, 1219–1225. [CrossRef]
20. Park, J.H.; Kim, D. Preparation and characterization of water-swellable natural rubbers. *J. Appl. Polym. Sci.* **2001**, *80*, 115–121. [CrossRef]
21. Ren, W.T.; Zhang, Y.; Peng, Z.L.; Zhang, Y.X. Investigation on the water-swelling properties of chlorinated polyethylene modified by in situ formed sodium acrylate. *Polym. Test.* **2004**, *23*, 809–816. [CrossRef]
22. Lang, F.; Li, S.; Du, F.; Wang, Z. Mechanical, Water-swelling, and Morphological Properties of Water-swellable Thermoplastic Vulcanizates Based on Polyvinyl Chloride/Crosslinked Sodium Polyacrylate/Chlorinated Polyethylene Blends. *J. Macromol. Sci. B* **2013**, *52*, 1322–1340. [CrossRef]
23. Zhang, Z.; Zhang, G.; Li, D.; Liu, Z.; Chen, X. Chlorohydrin water-swellable rubber compatibilized by an amphiphilic graft copolymer. II. Effects of PVA-g-PBA and CPA on water-swelling behaviors. *J. Appl. Polym. Sci.* **1999**, *74*, 3145–3152. [CrossRef]
24. Zhang, Z.; Zhang, G.; Wang, C.; Liu, D.; Liu, Z.; Chen, X. Chlorohydrin water-swellable rubber compatibilized by an amphiphilic graft copolymer. III. Effects of PEG and PSA on water-swelling behavior. *J. Appl. Polym. Sci.* **2001**, *79*, 2509–2516. [CrossRef]
25. Sae-oui, P.; Sirisinha, C.; Thepsuwan, U. Dependence of mechanical and aging properties of chloroprene rubber on silica and ethylene thiourea loadings. *Eur. Polym. J.* **2007**, *43*, 185–193. [CrossRef]
26. Nakason, C.; Nakaramontri, Y.; Kaesaman, A.; Kangwansukpamonkon, W.; Kiatkamjornwong, S. Synthesis and characterization of water swellable natural rubber vulcanizates. *Eur. Polym. J.* **2013**, *49*, 1098–1110. [CrossRef]
27. Zohuriaan-Mehr, M.J.; Kabiri, K. Superabsorbent Polymer Materials: A Review. *Iranian Polymer J.* **2008**, *17*, 451–477.
28. Tan, J.S.; Shen, S.L.; Zhou, A.; Wang, Z.N.; Lyu, H.M. Laboratory evaluation of long-term sealing behaviors of two water-swelling materials for shield tunnel gasket. *Constr. Build. Mater.* **2020**, *249*, 118711. [CrossRef]
29. Polgar, L.M.; Fallani, F.; Cuijpers, J.; Raffa, P.; Broekhuis, A.A.; van Duin, M.; Picchioni, F. Water-swellable elastomers: Synthesis, properties and applications. *Rev. Chem. Eng.* **2018**, *35*, 45–72. [CrossRef]
30. You, K.M.; Park, S.S.; Lee, C.S.; Kim, J.M.; Park, G.P.; Kim, W.N. Preparation and characterization of conductive carbon nanotube-polyurethane foam composites. *J. Mater. Sci.* **2011**, *46*, 6850–6855. [CrossRef]
31. Liu, C.; Ding, J.; Zhou, L.; Chen, S. Mechanical properties, water-swelling behavior, and morphology of water-swellable rubber prepared using crosslinked sodium polyacrylate. *J. Appl. Polym. Sci.* **2006**, *102*, 1489–1496. [CrossRef]
32. Ayres, E.; Oréfice, R.L.; Yoshida, M.I. Phase morphology of hydrolysable polyurethanes derived from aqueous dispersions. *Eur. Polym. J.* **2007**, *43*, 3510–3521. [CrossRef]
33. Brown, R.P. *Natural Ageing of Rubber—Changes in Physical Properties over 40 Years*; iSmithers Rapra Publishing: Shawbury, UK, 2000.
34. Kömmling, A.; Jaunich, M.; Pourmand, P.; Wolff, D.; Gedde, U.W. Influence of Ageing on Sealability of Elastomeric O-Rings. *Macromol. Symp.* **2017**, *373*, 1600157. [CrossRef]
35. Kömmling, A.; Jaunich, M.; Wolff, D. Effects of heterogeneous aging in compressed HNBR and EPDM O-ring seals. *Polym. Degrad. Stab.* **2016**, *126*, 39–46. [CrossRef]
36. Kömmling, A.; Jaunich, M.; Wolff, D. Revealing effects of chain scission during ageing of EPDM rubber using relaxation and recovery experiment. *Polym. Test.* **2016**, *56*, 261–268. [CrossRef]

37. Cortlever, N.G. *Geolock, Plastic HDPE-Liner for Vertical Cut-Off Barriers around Landfill*; Geotechnics Holland: Amsterdam, The Netherlands, 1995.
38. Manassero, M.; Pasqualini, E. Ground polluant containment barriers. In Proceedings of the Mediterranean Conference on Environmental Geotechnology, Cesme, Turkey, 25–27 May 1992; pp. 195–204.
39. Manassero, M.; Fratalocchi, E.; Pasqualini, E.; Spanna, C.; Verga, F. Containment with vertical cutoff walls. In *Geoenvironment 2000: Characterization, Containment, Remediation, and Performance in Environmental Geotechnics*; ASCE: Reston, VA, USA, 1995; pp. 1142–1172.
40. *ASTM D698*; Standard Test Methods for Laboratory Compaction Characteristics of Soil Using Standard Effort (12,400 ft-lbf/ft3 (600 kN-m/m^3)). ASTM: West Conshohocken, PA, USA, 2012.
41. *ASTM D2487*; Standard Practice for Classification of Soils for Engineering Purposes (Unified Soil Classification System). ASTM: West Conshohocken, PA, USA, 2018.
42. Yang, Y.L.; You, X.Y.; Chen, J.N.; Fu, X.L.; Du, Y.J. Hydraulic conductivity of novel geosynthetic clay liner to bauxite liquor from China: Modified fluid loss test evaluation. *J. Environ. Manag.* **2022**, *316*, 115208. [CrossRef]
43. *ASTM E70*; Standard Test Method for pH of Aqueous Solutions with the Glass Electrode. ASTM: West Conshohocken, PA, USA, 2015.
44. *ASTM D1125*; Standard Test Method for Electrical Conductivity and Resistivity of Water. ASTM: West Conshohocken, PA, USA, 2014.
45. *ASTM D3616*; Standard Test Method for Rubber—Determination of Gel, Swelling Index, and Dilute Solution Viscosity. ASTM: West Conshohocken, PA, USA, 2014.
46. *ASTM C143*; Standard Test Method for Slump of Hydraulic Cement Concrete. ASTM: West Conshohocken, PA, USA, 2015.
47. Petr, H.; Zdenka, V.; Petr, D. Water-swellable rubbers containing powdery poly(acrylamide) hydrogel. *Macromol. Mater. Eng.* **1997**, *245*, 203.
48. Wang, Z.N.; Shen, S.L.; Zhou, A.; Lyu, H.M. Experimental investigation of water-swelling characteristics of polymer materials for tunnel sealing gasket. *Constr. Build. Mater.* **2020**, *256*, 119473. [CrossRef]
49. Liao, S.Q.; Lin, H.J.; She, X.D.; Liao, J.H. Research and preparation of curing water-swelling natural rubber. *Spec. Purpose Rubber Prod.* **2009**, *30*, 5–8. (In Chinese)
50. Lee, W.F.; Wu, R.J. Superabsorbent polymeric materials. I. Swelling behaviors of crosslinked poly (sodium acrylate-co-hydroxyethyl methacrylate) in aqueous salt solution. *J. Appl. Polym. Sci.* **1996**, *62*, 1099–1114. [CrossRef]
51. Liu, J.C.; Duan, Y.S. Preparation and properties of water swellable water-swelling polyurethane elastomer. *China Elastomerics* **2010**, *20*, 9–12. (In Chinese)
52. Ma, J.; Wang, T.W. Preparation and characterization of water-absorbing water-swelling polyurethane foam composites with microsized sodium polyacrylate particles. *J. Appl. Polym. Sci.* **2018**, *135*, 46702. [CrossRef]